



# Numerical and experimental investigation of a 3D-printed PCU patient-specific cranial implant

Gregorio Pisaneschi<sup>1</sup> · Mattia Mele<sup>1</sup> · Andrea Zucchelli<sup>1</sup> · Maurizio Fiorini<sup>2</sup> · Giampaolo Campana<sup>1</sup> · Emanuela Marcelli<sup>3</sup> · Achille Tarsitano<sup>4,5</sup> · Elisabetta Lucchi<sup>4,5</sup> · Laura Cercenelli<sup>3</sup>

Received: 30 January 2023 / Accepted: 28 April 2023 / Published online: 10 May 2023  
© The Author(s) 2023

## Abstract

Arburg plastic freeforming (APF) technology allows for fabricating patient-specific implants (PSIs) in a hospital environment using medical-grade thermoplastic polymers. Among these materials, poly(carbonate-urethane) (PCU) is of great relevance since it is characterised by excellent biocompatibility. This study explores the opportunity to realise a patient-specific cranial plate via APF. First, a Finite Element model (FEM) of the implant under compressive loads is developed and validated using a quasi-isotropic material. Then, this model is used for Finite Element Analysis (FEA) considering Technical Datasheet (TDS) material properties and those measured on 3D-printed specimens, by Three-Point Bending (TPB) tests. Finally, a PCU PSI is fabricated through APF and tested under static loads to validate the consistency of the numerical results. Considering TDS properties, the FEA results indicate that PCU can be used for the manufacturing of this device. Nonetheless, the TPB tests show that the material suffers from a loss of mechanical properties. Using these properties, the displacements calculated via FEA exceed the admissible values for the application. A further decrease in stiffness is observed in the manufactured plate. Overall, findings suggest that PCU can be a viable material to be printed by APF technology for fabricating craniofacial PSIs, with the advantage of minor stress concentration in critical points of the implant if compared with polyetheretheretherketone (PEEK). However, further studies are necessary to effectively represent the effects of 3D printing in the FEMs used for structural validation and design optimisation.

**Keywords** Additive manufacturing · Arburg plastic freeforming · Reconstructive surgery · Patient-specific implants · PCU · Finite element analysis

---

✉ Gregorio Pisaneschi  
gregorio.pisaneschi@unibo.it

Mattia Mele  
mattia.mele@unibo.it

Andrea Zucchelli  
a.zucchelli@unibo.it

Maurizio Fiorini  
maurizio.fiorini@unibo.it

Giampaolo Campana  
giampaolo.campana@unibo.it

Emanuela Marcelli  
emanuela.marcelli@unibo.it

Achille Tarsitano  
achille.tarsitano2@unibo.it

Laura Cercenelli  
laura.cercenelli@unibo.it

<sup>1</sup> Department of Industrial Engineering (DIN), University of Bologna, Viale del Risorgimento, 40136 Bologna, Italy

<sup>2</sup> Department of Civil, Chemical, Environmental and Materials Engineering (DICAM), University of Bologna, Via Terracini 28, 40131 Bologna, Italy

<sup>3</sup> eDIMES Lab, Department of Medical and Surgical Sciences (DIMEC), University of Bologna, Via Massarenti 9, 40138 Bologna, Italy

<sup>4</sup> Department of Biomedical and Neuromotor Sciences (DIBINEM), University of Bologna, Via Massarenti 9, 40138 Bologna, Italy

<sup>5</sup> Oral and Maxillo-facial Surgery Unit (IRCCS), Azienda Ospedaliero-Universitaria di Bologna, Via Massarenti 9, 40138 Bologna, Italy

## 1 Introduction

Cranioplasty is a surgical reconstructive procedure to restore the structural integrity of cranial defects that may result from craniectomy following cerebral infections, head trauma, or bone resection for intracranial tumours [1].

The main clinical challenges in the reconstruction of craniofacial bone defects are the achievement of precise implant fit and adequate mechanical resistance, as well as the improvement of the aesthetics, quality of life, and psychological well-being of the patient [2].

Cranial implant design has to consider two important aspects: biocompatibility and customization to the patient. Biocompatibility is guaranteed by appropriate material selection. The customization is achieved by processing the patient diagnostic imaging data, which allows a precise representation of the skull trauma with the surrounding bone tissue, and the subsequent design and fabrication of Patient-Specific Implants (PSIs) matching the patient's unique anatomy [3–5]. In the following sections, the most recent advancements in the design and manufacturing of PSIs are briefly summarised, with an emphasis on polymeric materials 3D printing, Finite Element Analysis (FEA) modelling and characterization.

### 1.1 Biomaterials

A large and growing body of literature has investigated biomaterials for craniofacial reconstruction, including metals, ceramics and polymers [6].

Particularly, polymers are highly attractive for craniofacial repair, due to their good processability and low cost in comparison to metals and ceramics. Unlike ceramics, which are brittle and are exclusively used for bone replacement, they are resilient. In addition, polymers have the advantage of being radiolucent, hence facilitating unobstructed post-operative clinical diagnoses as opposed to imaging artefacts caused by metallic implants [6]. Table 1 summarises the mechanical properties of the

main biomaterials used for craniofacial PSIs, namely Titanium, Polyether Ether Ketone (PEEK), Polyetherketoneketone (PEKK), Ultra-High-Molecular-Weight Polyethylene (UHMWPE) and Polymethyl methacrylate (PMMA). The properties of poly(carbonate-urethane) (PCU), which is the object of this study, and natural cranial bone are also included.

PMMA was one of the first synthetic materials used for biomedical applications [11] and finds applications also in cranioplasty. In spite of their diffusion, PMMA implants show poor osseointegration properties [12].

UHMWPE is one of the most widely used materials in cranioplasty. This polymer is characterized by low density, non-toxicity and high bio-affinity [13]. Nevertheless, its low mechanical properties make it less effective than other polymers in replicating the mechanical behaviour of the cranial bone.

In recent years, biocompatible high-performance polymers like PEEK and PEKK have gained popularity in craniofacial reconstructions [3, 14–16] and orthopaedic applications [17]. They are chemically inert with high thermal stability and mechanical properties comparable to bone, thus offering an excellent alternative to metallic biomaterials in craniomaxillofacial reconstructive surgeries. Both polymers can be sterilized, facilitating their use in healthcare applications. As a drawback, the high stiffness of these polymers may cause high stresses acting on the cranial bone.

Other promising polymers are the PCU, which are commercially available in medical-grade formulation (e.g. Bionate@PCU, DSM Medical DSM Biomedical Inc., Berkeley, CA, US) and have been extensively characterized in the body of the literature [9, 18–20]. These polymers are highly suitable for use in orthopaedic implants since they offer a unique combination of toughness, durability, flexibility, biocompatibility, and bio-stability [21]. The potential advantages of the use of PCU for craniofacial PSIs are discussed in more detail in Sect. 2.

**Table 1** Mechanical properties of the main materials of interest for cranial reconstruction

Material	Density	Young modulus	Ultimate tensile strength	Poisson's ratio	References
–	$\left(\frac{g}{cm^3}\right)$	$(GPa)$	$(MPa)$	–	–
Titanium	4.42	110.00	1300	0.3	[7]
PEKK	1.31	3.80	110	0.35	[7]
PEEK	1.3	3.50	105	0.4	[7]
UHMWPE	0.94	1.10	41	0.46	[7]
PMMA	1.18	3.00	72	0.38	[8]
PCU 75D	1.22	0.89	63	0.49	[9]
Cranial bone	1.8	5.38	43	–	[10]

## 1.2 Manufacturing of cranial plates

Traditional manufacturing techniques for the production of PSIs such as injection moulding [22] and casting [23] are time-consuming, expensive and subjected to shrinkage control [24]. Also, the adoption of moulds does not allow for the patient-oriented customisation of the geometries.

Several studies investigated milling machining for manufacturing implants used in cranial reconstructions [3, 25]. This approach allows for greater flexibility but determine a significant waste of material due to milled chips.

In the last decade, greater attention has been given to the use of Additive Manufacturing (AM), also known as Three-Dimensional Printing (3DP), in medicine. The applications of these processes in the field include anatomical models for preoperative planning, surgical guides, and prosthetic devices [26–32]. Particularly in the context of cranioplasty, many experiences have been reported on the fabrication of customized cranial implants using 3D printing [33, 34].

Among AM processes, Laser Powder Bed Fusion (LPBF) is the most widely adopted for fabricating PSIs since it can handle a number of biocompatible thermoplastics and metal alloys. LPBF of PEEK parts was first proposed by Schmidt et al. [35]. Later the EOS P800 3D printer (EOS, Electro-Optical Systems GmbH, Krailling, Germany) was launched for additive manufacturing of parts from PEEK powders using a high-temperature laser sintering technology [36]. However, this technology, requires expensive powders, the handling of which poses a risk in a hospital environment.

Recent studies have demonstrated the opportunity to use filament-based material extrusion 3D printing, usually referred to as Fused Filament Fabrication (FFF), to produce customized PEEK implants. This result is achieved using medical-grade PEEK filaments and high-temperature FFF 3D printers explicitly tailored for medical PEEK applications [34, 37–39]. Compared to LPBF technology, FFF offers the advantages of lower initial machine costs, easier operability and cleaner working environment [40].

However, this process must face significant challenges, such as the thermal management during the PEEK printing process, the residual stress build-up, and the anisotropic behaviour of the FFF 3D-printed PEEK implants. Indeed, due to the layer-by-layer fabrication method, the shrinkage contributes to weak interlayer bonding and, as a result, induces structural failures at the interface between the layers [41]. FFF also suffers from a limited number of processable polymers. This is due not only to the need for fabricating filament but also to the constraints in terms of material stiffness [42]. Specifically, elastic materials are prone to buckling of the filament entering the extruder [43].

To surpass these limitations, several AM processes using granulated pellet as a feedstock have been developed [44, 45]. Among these processes, Arburg Plastic Freeforming

(APF) attracted a considerable attention. This process adopts a unique droplet-based deposition strategy inspired by injection moulding techniques. The granulate material is firstly melted by means of a reciprocating screw. Then, the polymer melt is pushed towards a deposition nozzle, which is sealed by a closure. Finally, a piezo actuator is used to open the nozzle intermittently so as to deposit small droplets of polymer melt on a moving building plate [46].

The increasing interest in this process is mainly due to the properties of manufactured parts. Specifically, previous studies demonstrated that this technology achieves higher accuracy, density and mechanical properties if compared to FFF [47, 48]. Moreover, the APF technology can allow for transforming an exceptionally wide range of polymers.

What is most important for applications in the biomedical field is the opportunity to use polymers which have previously had regulatory approval for use in medical devices [49]. In fact, the process does not require intermediate transformations of the material such as filament extrusion, which can invalidate the certification [50]. This extends the opportunity to test with new materials and provide patients with custom implants [51, 52].

An example of medical application of the APF system was presented by Welsh et al., who proposed an innovative drug-releasing vaginal ring by medical-grade Thermoplastic Polyurethane (TPU) [53]. Zhang et al. used this technology to print edible on-demand drug realising solid dosage forms [54]. Hentschel et al. investigated a medical grade PMMA for implant applications. Specifically, the authors provided a method for the definition of process parameters and a characterisation of the material [50]. According to the Arburg APF sales department, many more applications of the technology for the manufacturing of patient-specific medical implants have recently emerged [55]. Nevertheless, information on these applications is not yet available in the literature.

To the authors' knowledge the AM processing of medical-grade polymers through the APF technology for fabricating PSIs remains quite under-investigated.

## 1.3 FEA modelling and characterization of cranial implants

To date, the design of craniofacial implants is carried out by operating surgeons based on clinical needs. In most cases, no mechanical analyses of the PSIs are performed, in spite of the great relevance of this aspect. The main reason is that an iterative experimental approach to mechanical design would be highly expensive and time-consuming due to the need for numerous tests and prototypes. As demonstrated by previous studies, numerical simulation by finite-element analysis (FEA) can be effectively used to optimise the mechanical design while limiting the cost of the design phase.

El Halabi et al. [56] developed a Finite Element Model (FEM) of a cranial implant incorporating a scaffold structure. The implant was manufactured in biocompatible PEEK through LPBF technology. The material used to fabricate the implant was preliminary characterized by means of Three-Point Bending (TPB) tests. Then, experimental tests were conducted on two cranial implant designs to observe their mechanical performance and validate the results of the FEA.

Garcia-Gonzalez et al. [57] developed a FEM of the head starting from magnetic resonance imaging data. Such a model comprises the scalp, skull, cerebral falx, cerebrospinal fluid, brain tissues and an implant replacing part of the skull. The model was then used to study the mechanical response under a wide range of impact conditions. Finally, numerical simulations were conducted to compare the mechanical response of PEEK and hydroxyapatite (HA) cranial implants.

Zhigang Wan et al. [58] used FEA to compare the resistance of four different skull implants made of PEEK and Titanium. Skulls and implants were considered isotropic, homogeneous and continuous linear elastomers.

Marcían [59] investigated the effects of implant thickness and material on deformation and stress distribution. An anatomically realistic model consisting of a human skull, cranial implant, mini-plates and micro-screws was manufactured and studied using non-linear FEA. The implant assembly model included the detailed geometries of the mini-plates and micro-screws and was simulated using a sub-modelling approach.

This paper provides a numerical and experimental investigation of a PCU patient-specific cranial implant produced through APF. First, a numerical model of the implant based on FEM was developed. This model was validated using a quasi-isotropic 3D printing process, namely Stereolithography Apparatus (SLA). Then, the FEM was applied to predict the static behaviour of PCU implants realised through APF. The PEEK cranial plate used for surgery was also simulated to compare the distribution of stress and displacements. To better represent the mechanical properties of the final component fabricated in PCU, an experimental campaign was carried out to characterise PCU specimens realised by APF. Finally, a PCU cranial plate was printed via APF and tested under

quasi-static loads. The results of experimental tests were compared to those predicted by FEA to highlight the limits of numeric analysis.

## 2 Methods

### 2.1 Design of the patient-specific implant

The present study investigates the retrospective case study of a patient requiring a reconstructive cranial plate. This case was treated at the Maxillofacial Surgery Unit of IRCCS Azienda Ospedaliera Universitaria di Bologna.

The patient-specific Computer-Aided Design (CAD) model of the cranial implant was generated starting from a high-resolution Computed Tomography (CT) imaging of the patient. Using image segmentation and subsequent surface reconstruction by Mimics Medical software (Materialise NV, Leuven, Belgium), the 3D model of the skull with the defect was reconstructed and saved in Standard Tessellation Language (STL) format. This model was used as a starting point to extract the cranial implant dimension and external contours. Then, the patient-specific reconstructive plate was designed to ensure the perfect matching between the implant and the host skull geometry. To this end, 3-Matic software by Materialise was used. The obtained patient-specific CAD model of the cranial implant is shown in Fig. 1, which summarises the entire design workflow.

For clinical purposes, pre-surgical models of the defective skull and the designed patient-specific cranial plate were 3D printed with SLA. Then, a PEEK plate printed via LPBF was implanted on the patient for replacing the injured skull. Figure 2 shows both the pre-surgical model and the PEEK cranial plate used for surgery.

It must be noted that this implant is designed manually using a dedicated CAD software, a process that might take days or even weeks. In the interim, the patient will need temporary brain protection, and eventually, a second surgery to replace the implant. To accelerate the implant design process and reduce waiting times for the patient, some recent studies have investigated the possibility of automatically creating an implant model from a CT scan using deep learning [60–62].

**Fig. 1** Design workflow of the patient-specific implant. **a** CT scan, **b** Image segmentation and skull model reconstruction, **c** Design of the patient-specific cranial plate, **d** export of the STL model

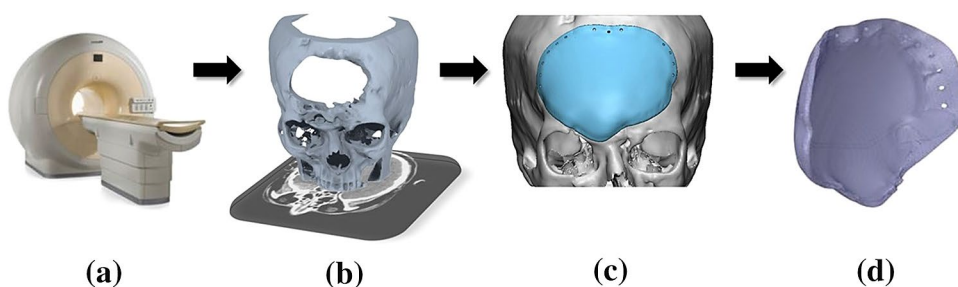


**Fig. 2** **a** Pre-surgical model of the skull coupled with **a** a prototype of the cranial plate made via SLA and **b** the final PEEK implant made by LPBF

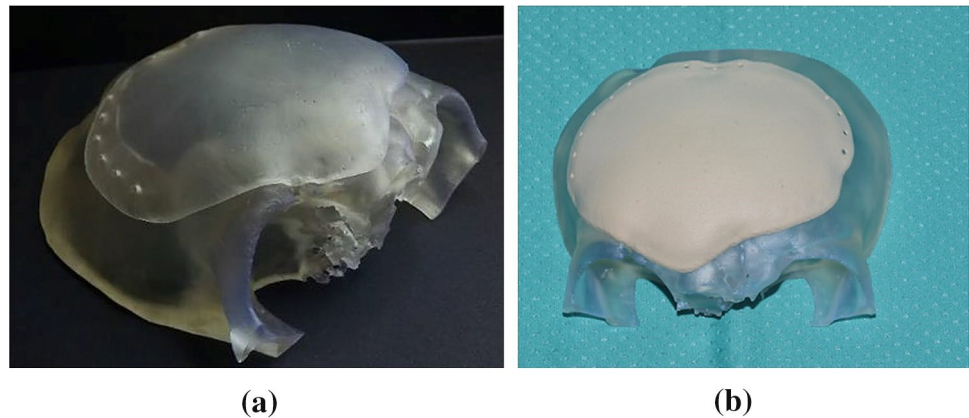


**Table 2** Mechanical and technological properties of the Bionate PCU 75D as reported in the manufacturer technical datasheet [63]

Property	Unit	Value	Test method
Density	g/cm <sup>3</sup>	1.22	ASTM D792
Water absorption	%	0.8	ASTM D750
Mould shrinkage, 4// disk	%	1.2	ASTM D955
Melt flow rate, 5000 g @ 224 °C	g/10 min	14	ASTM D1238
Hardness, Shore D		73D	ASTM D2240
Ultimate tensile strength	MPa	63.23	ASTM D1708
Ultimate elongation	%	241	ASTM D1708
Flexural modulus, Secant 1.00%	MPa	1.792%	ASTM D790
Flexural stress, at 5.00%	MPa	70.3%	ASTM D791
Recommended extrusion temperature	°C	190–232	
Drying temperature	°C	82	
Dry time	hours	4	

## 2.2 Materials

As discussed in Sect. 1, numerous biocompatible materials can be considered for fabricating PSIs in craniomaxillofacial applications. The present study focuses on PCU. Specifically, the medical-grade Bionate 75D PCU is investigated. The physical, mechanical and processing properties of this material are summarised in Table 2 [63].

Medical-grade Bionate®PCU polymers are currently being used in a wide range of applications, including neurostimulation, vascular, artificial heart, cardiac assist and diagnostic devices. Because of their exceptional load-bearing capability and bio-stability, these materials are also extensively used for orthopaedic applications such as hip and knee joints and spinal motion preservation devices [64–66].

In addition, PCU exhibits a highly time-dependent behaviour characterized by viscoelastic properties. Stiffening of the material with increasing strain rate has been observed for Bionate, with a reduction in the strain at break [9]. This

interesting elastomeric behaviour can help to absorb impact energy and to avoid stress concentration, which may affect a cranial plate after implantation.

As a drawback, PCU is highly hygroscopic. Water absorption has a significant influence on both dimensional accuracy and mechanical properties. In fact, previous studies reported that conditioning considerably reduces the elastic modulus and Ultimate Tensile Strength (UTS) of Bionate 75D PCU [9]. Unlike high-resistant polymers such as PEEK and PEKK, PCU can be printed at relatively low temperatures (see Table 2). This feature is highly beneficial as it reduces the complexity of the manufacturing process and the distortions when the part is cooled at room temperature.

## 2.3 Manufacturing

Preliminary samples of the cranial plate were 3D printed by SLA using a Form 3 printer by Formlabs. CLEAR FLG-PWH04 standard resin [67] was used for the process and the material was post-processed under a 1.25 mW/cm<sup>2</sup> LED light with a 405 nm wavelength for 60 min at 60 °C. This material is quasi-isotropic and is thus used in the next sections to validate the FEM.

To anchor the cranial plate for mechanical testing, the support base shown in Fig. 3 was manufactured with a Prusa i3 MK3 using carbon fibre-reinforced polyamide PAHT CF15. This material was chosen as it offers higher stiffness than those used for manufacturing the cranial plate. Cylindrical PAHT CF15 specimens (20 mm in diameter and 20 mm in height) were preliminarily printed to characterise the material under experimental compression tests.

The Bionate 75D PCU parts were manufactured using an APF 2X-200K printer machine by ARBURG GmbH. Starting with a set of parameters recommended by Arburg's expertise, print settings were determined by optimising the Drop Aspect Ratio (DAR) and nozzle temperature [68]. The DAR was fine-tuned by printing several parallelepipeds of 20 × 20 × 5 mm as those shown in Fig. 4 until satisfactory



Fig. 3 Support base used to anchor the cranial plate for testing

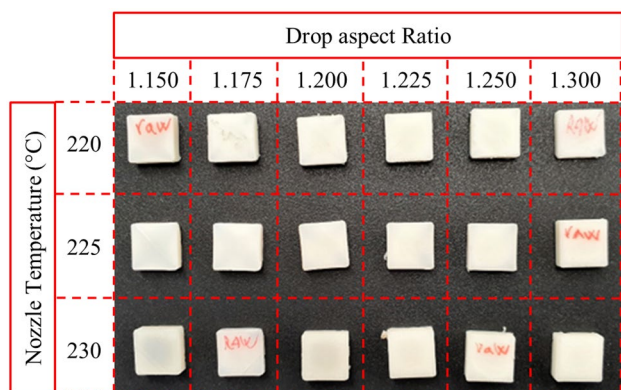


Fig. 4 Benchmark parallelepipeds at different combinations of DAR and nozzle temperature

Table 3 Process parameters used for APF of PCU

Parameter	Unit	Value
Nozzle temperature	°C	230
Temperature region 1	°C	225
Temperature region 2	°C	180
Build chamber temperature	°C	120
DAR	–	1.3
Contouring speed	mm/s	9
Hatching speed	mm/s	36
Travelling speed	mm/s	150

results in terms of accuracy and filling were achieved. The nozzle and chamber temperatures were set to achieve a good layer adhesion without degrading the material and preventing oscillations of the DAR during the printing due to a lower viscosity. The printing parameters used for PCU manufacturing are summarised in Table 3. Due to its high hygroscopicity, the material was dried, as suggested by the datasheet [63], at 80 °C for 8 h in a vacuum autoclave.



Fig. 5 PCU cranial plate printed by APF with 50% support density

To evaluate the mechanical characteristics of the PCU printed by APF, TPB specimens of dimensions 80 × 10 × 4 mm were printed and tested according to the ISO 178 standard.

The PCU cranial plate was printed in the orientation shown in Fig. 5. This build orientation was chosen as it allows to avoid support structures on the concave surface, i.e. on the region facing the brain. It is worth mentioning that, due to the surface curvature, support structures are unavoidable. To date, no studies reported information about the compatibility between PCU and solvable support materials. Therefore, the support structures were realized in PCU and manually removed at the end of the printing job. Two replicas of the cranial plate were printed with different support designs. Specifically, support structures with infill densities of 25% and 50% were tested.

### 2.4 Finite element model

All the steps of the FEA have been carried out using Ansys®Mechanical software. For the scope of these analyses, a solid geometry has been reconstructed starting from the STL model of the cranial plate obtained as described in Sect. 2.1 and shown in Fig. 1. To ensure a suitable model for simulation, the mesh exported by 3Matic was repaired, smoothed and homogenized by means of the SpaceClaim package by Ansys®. Then, the solid geometry was generated according to the workflow schematically shown in Fig. 6. First, the curvature of the implant was reconstructed using 12 auto-generated patches (Fig. 6b). Second, the peripheral contact region to the support base was manually defined (Fig. 6c). Then, the contact area with the punch was obtained by a normal projection along the displacement direction (Fig. 6d). Finally, the 1.5 mm diameter holes, used for fixing the plate, were modelled and the countersinks were added (Fig. 6e, f).

The FEM is designed to replicate the setup of the experimental compression test. The implant is in contact with the support base, which simulates the patient’s cranium. The geometry of the support base was obtained by vertically extruding the contact surface to a horizontal plane.

**Fig. 6** Workflow to obtain a solid geometry for FEA. **a** Starting STL model, **b** patches generation, **c** definition of the contact region to the support base, **d** definition of the punch contact region, modelling of **e** holes and **f** countersinks

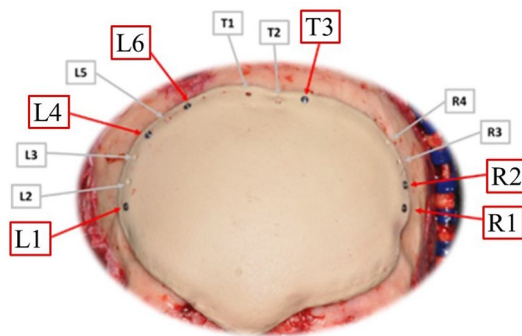
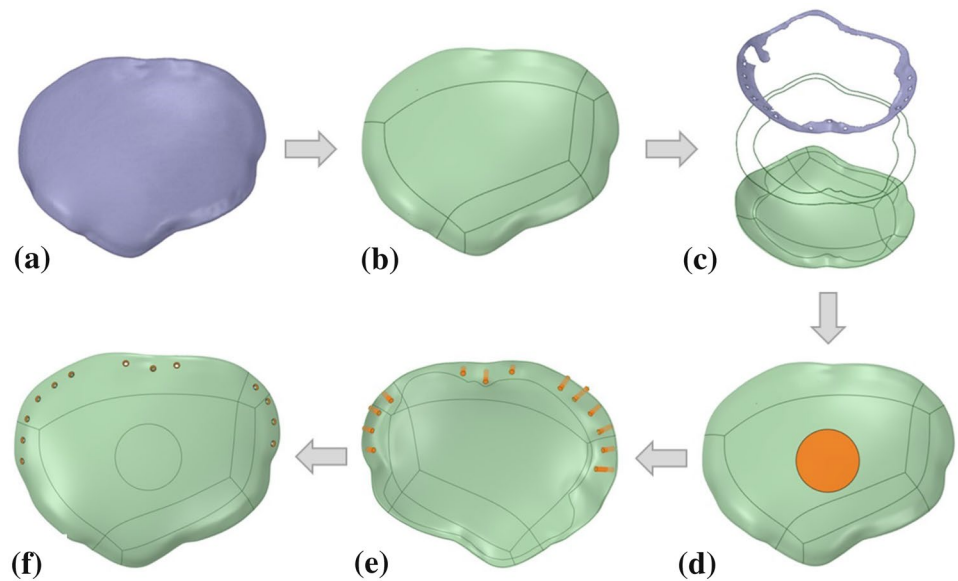


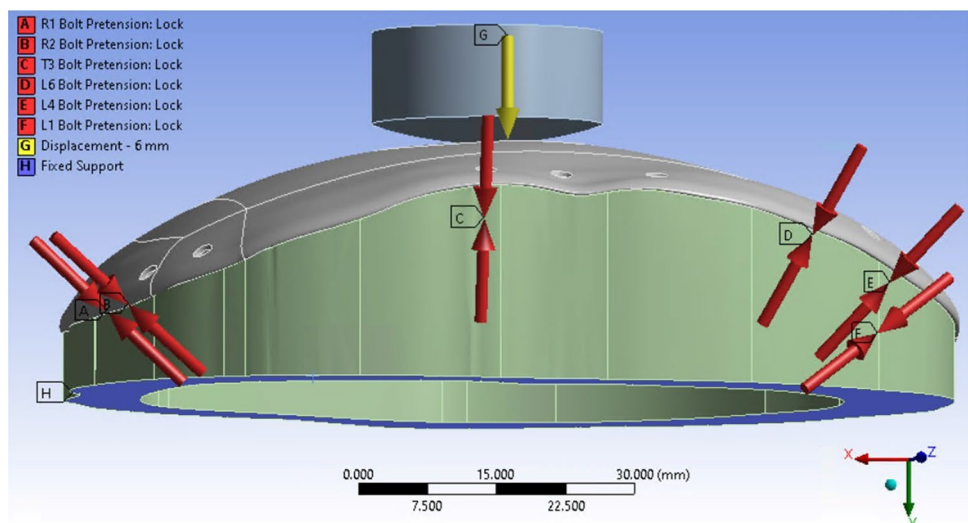
**Fig. 7** Intraoperative picture of the cranial plate. The screws used for anchoring are highlighted in red colour

It is worth mentioning that not all the holes shown in Fig. 6e were used in the real application. In fact, more holes than necessary are realized so as to allow choice during surgery. In the investigated case, the implant was anchored intraoperatively using the six screws highlighted in Fig. 7.

As will be detailed in the following sections, the experimental tests were carried out by applying a compressive load to the cranial plate by means of a punch. The punch was designed as a cylinder of 25 mm diameter ending with a spherical cap of 40 mm radius. Figure 8 shows the complete finite-element setup of the compressive test.

Preliminary FEAs showed that the mechanical behaviour of the 3D-printed support base can be effectively approximated by means of a Mooney–Rivlin model with three parameters. These parameters, were obtained from

**Fig. 8** FEM setup of the compression test



compression tests performed on the cylindrical fibre-reinforced polyamide specimens.

Other materials used in the FEM are titanium for the screw and steel for the punch. The properties of these materials were retrieved from the Granta material library included in Ansys®. Finally, the PEEK manufactured via LPBF was modelled using the material parameters presented by [69].

A convergence test was performed by iteratively refining the mesh size. The resulting mesh consists of 243.151 quadratic tetrahedrons (TET10). Since a concentration of stresses is expected nearby screw holes, the mesh was locally refined to achieve a more accurate result. Figure 9 shows a detail of the local element size nearby the screw holes. The mesh was also refined in the contact regions between the base, the plate and the punch.

A fixed constraint was applied to the bottom surface of the support base. Frictional contacts were imposed at the plate's interfaces with the base and the punch. Six beam connections were used to model the six anchoring screws shown in Fig. 7.

The static simulation consists of two steps. In the first step, a pre-load equal to 5 N is applied to the beam connections to replicate the tightening of the screws during the assembly of the experimental setup. Then, a displacement of 6 mm along the *Y*-axis (see Fig. 8) is applied to the punch. The corresponding load acting on the fixed surface of the support plane is acquired to draw the load versus deformation curves.

The stress and deformations of the implant were evaluated in correspondence to specific values of load reported by previous literature. The first value is equal to 50 N, which corresponds to the scenario in which the head is in

resting on a flat surface [8]. The second reference value is equal to 500 N and, according to [58], is representative of a severe impact.

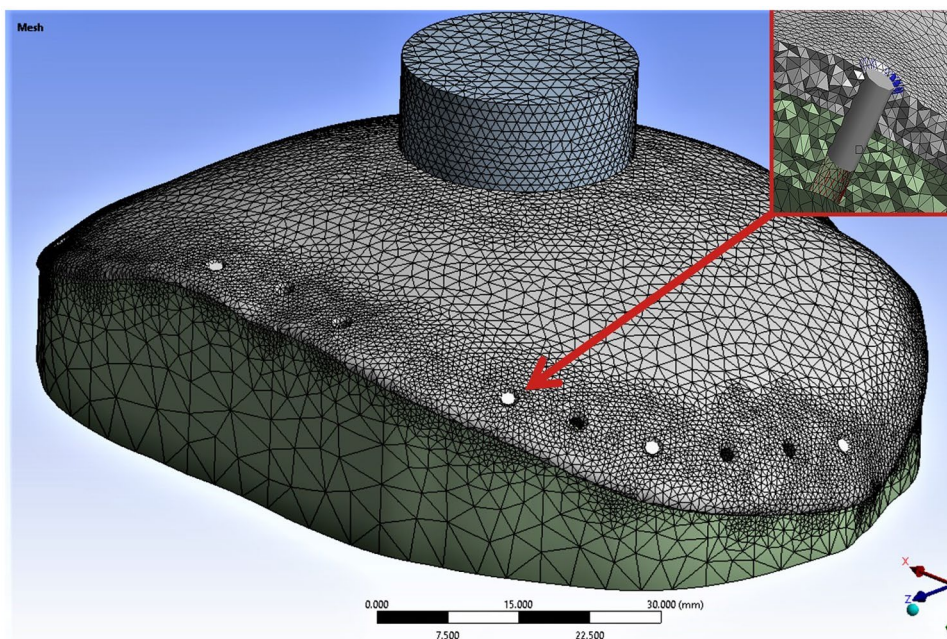
## 2.5 Characterisation of the 3D-printed PCU

For the scope of FEA, the properties of the PCU were initially set equal to those indicated by the manufacturer in the Technical Datasheet (TDS) and reported in Table 2. Then, a second simulation was performed by considering the mechanical properties derived from the experimental TPB tests performed on the 3D-printed specimens. Before the tests, the specimen density was measured by means of the gravimetric buoyancy technique which utilizes Archimedes' principle. TPB tests were performed on an Instron 5966 equipped with a 10 kN load cell. According to the ISO 178 standard guidelines, the support span was 64 mm and the test speed was 2 mm/min. Three repetitions of the test were performed. In both cases, a bilinear model with secant at 1% and 5% strain was used to calculate flexural modulus. The Poisson coefficient for all PCU set of properties was taken from the literature [70] and set to 0.49.

A picture of the TPB tests on PCU specimens is shown in Fig. 10a. The TPB tests were interrupted ahead of failure since the deformation of the specimens was such to make them slip away from the supports. Flexural stress and strain were calculated according to the ISO 178 standard.

To verify the accuracy of the material model, a FEA replicating the TPB was performed. This analysis is carried out using two symmetry conditions, as shown in Fig. 10b.

**Fig. 9** Mesh used for simulation with a focus on the local refinement nearby the screw holes





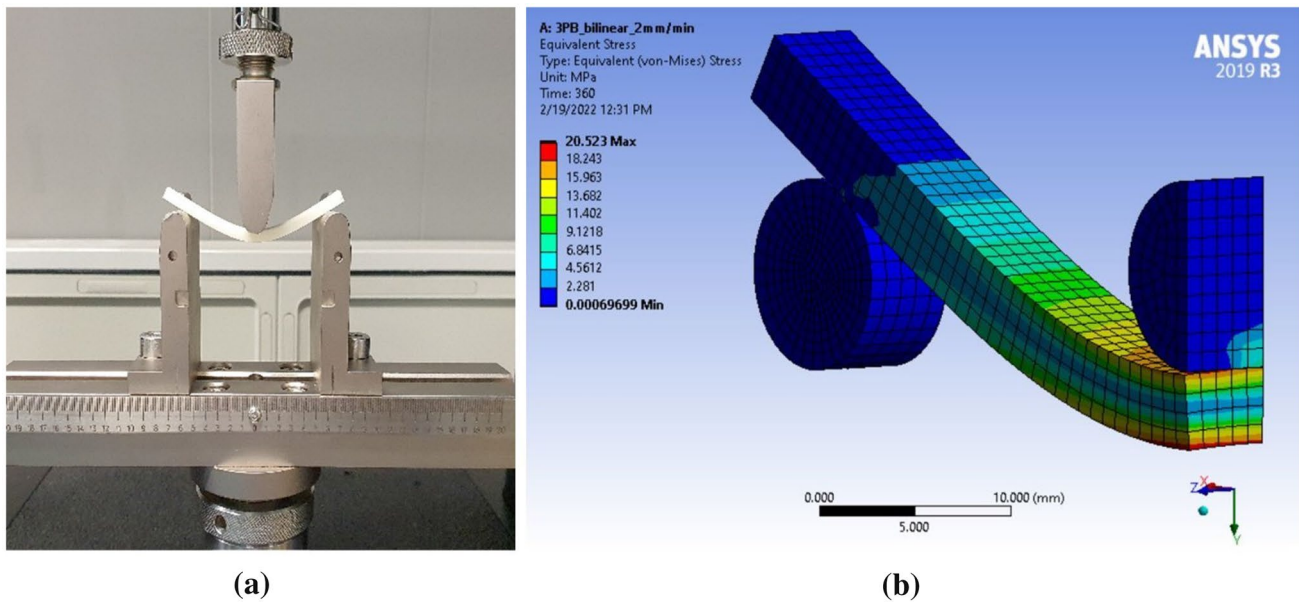


Fig. 10 a Picture of the TPB tests and b corresponding FEA

### 2.6 Mechanical tests on the implants

All the mechanical tests were carried out on an INSTRON electro-mechanical Universal machine equipped with a 10 kN load cell, at a 2 mm/min speed. A maximum displacement of 6 mm was imposed on the punch, which was initially in contact with the tested part.

As mentioned in the previous sections, a preliminary mechanical test on the cranial plate printed via SLA was carried out to validate the FEA model presented in Sect. 2.4. Specifically, the replica of the implant manufactured by SLA was tested under a maximum load of 500 N. Mechanical properties of the Formlabs SLA resin reported in the technical datasheet [67] were used for bilinear modelling of the material.

The support base was coupled using screws to a metallic plate anchored to the testing machine. The SLA cranial plate was mounted on the support base with surgical screws tightened with a torque wrench. Figure 11 shows a picture of the complete setup.

The same compressive test was carried out on the two PCU plates manufactured by APF.

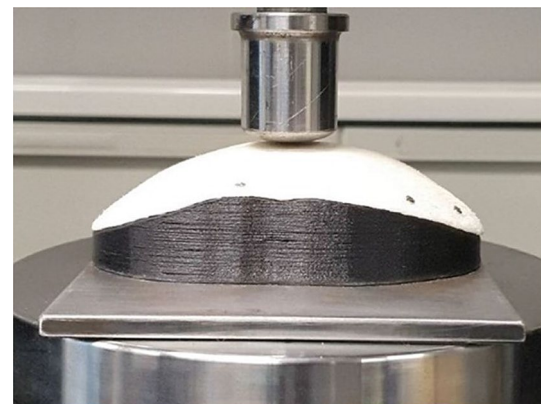


Fig. 11 Picture of the mechanical test setup

Table 4 Mechanical properties of the PCU

Propriety	TDS [63]	3D-printed TPB	Percent difference
Flexural modulus, secant 1% (MPa)	1792	518 ± 16	71.09%
Flexural stress, @ 5% Deflection (MPa)	70.3	18.62 ± 0.10	73.54%

## 3 Results

### 3.1 Three-point bending tests on 3D-printed PCU

The physical and mechanical properties of the 3D-printed PCU observed by TPB tests are summarized in Table 4. This table also reports data from the PCU TDS for comparison.

The experimental data in Table 4 were used to implement a bilinear model of the PCU material, which is then used for the FEA shown in Fig. 10b. Figure 12 compares a typical load–displacement curve obtained by the experimental TPB tests with that calculated via FEA. The slight difference is

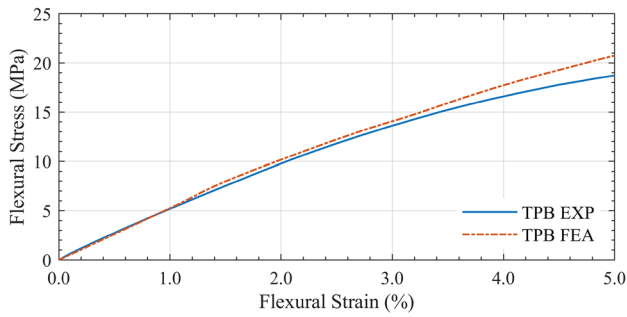


**Fig. 12** Comparison between experimental (EXP) TPB observations and results calculated via FEA using a bilinear model of the material

most likely due to the bilinear approximation which gives a stiffer behaviour for higher deformations.

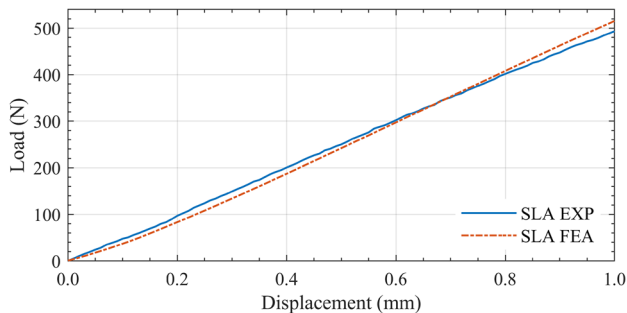
### 3.2 Validation of the finite-element analysis

Figure 13 shows the force measured in the experimental compression test on the SLA resin-printed cranial implant and the response force computed by FEA.

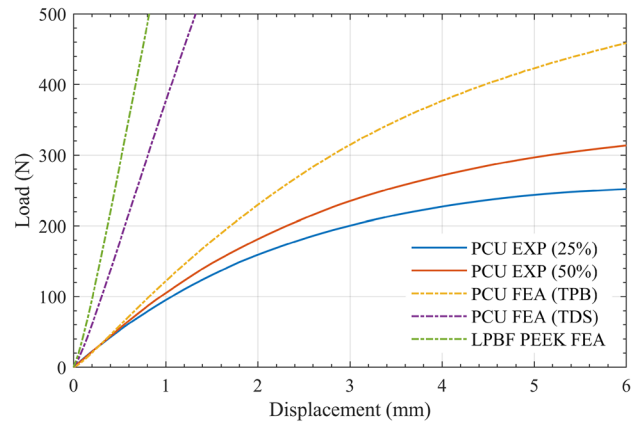
### 3.3 Compression tests on PCU implant

Figure 14 shows the different load–displacement curves of the PCU cranial plate. Particularly, the force measured in the experimental tests performed on the APF-printed PCU plates with 25% and 50% density of support structures are plotted. Figure includes also the results obtained by FEA. These comprise the simulation with material properties from TDS and those obtained by TPB tests. Also, the results of the FEA carried out considering the characteristics of PEEK printed via LPBF are shown.

The distributions of total deformation and equivalent von Mises stress of the FEAs are shown in 15. Specifically, results obtained considering the properties of LPBF PEEK, TDS PCU and 3D-printed TPB PCU are reported. A red label is used to highlight the points of maximum stress and



**Fig. 13** Comparison between experimental results (EXP) of compression test on SLA cranial plate and corresponding FEA results



**Fig. 14** Results of compression tests on PCU cranial plate printed by APF and FEA results on PCU and PEEK

deformation. These results are evaluated for the maximum load considered, 500 N, in case of LPBF PEEK and TDS PCU. In the case of 3D-printed TPB PCU, are evaluated at the maximum displacement considered, 6 mm, at which correspond 459 N of load.

## 4 Discussion

As shown in Fig. 13, the results of compression tests on the SLA resin plate are in good accordance with the values calculated by FEA. The maximum difference between the two curves is equal to 22 N. The curves highlight an almost linear relation between the compressive load and the displacement of the application point. The FEM appears slightly stiffer at higher deformations. This is arguably attributable to the bilinear modelling of the material characteristic. Overall, these findings allow for validating the results of the FEA, which is thus used for the following analyses.

This FEM then used to calculate the mechanical behaviour of the implant considering TDS characteristics of the PCU and those of the implanted solution, namely PEEK by LPBF. As shown in Fig. 15, in both these simulations, the maximum stress is located nearby screw holes. This finding is expected since holes are stress concentrators [59].

Tables 5 and 6 report the equivalent von Mises stress acting on the holes at 50 N and 500 N, respectively. It can be seen that the use of PCU determines a reduction of stresses on the screw holes. This is attributable to the elastomeric behaviour of this material, which determines a more efficient redistribution of deformation energy. This finding highlights a potential benefit of the adoption of PCU for cranial implants.

On the other hand, the curves shown in Fig. 14 highlight that the adoption of this material determines a less rigid behaviour of the cranial plate if compared to the implanted

**Fig. 15** Maps of von Mises equivalent stress (MPa) and total deformation (mm)

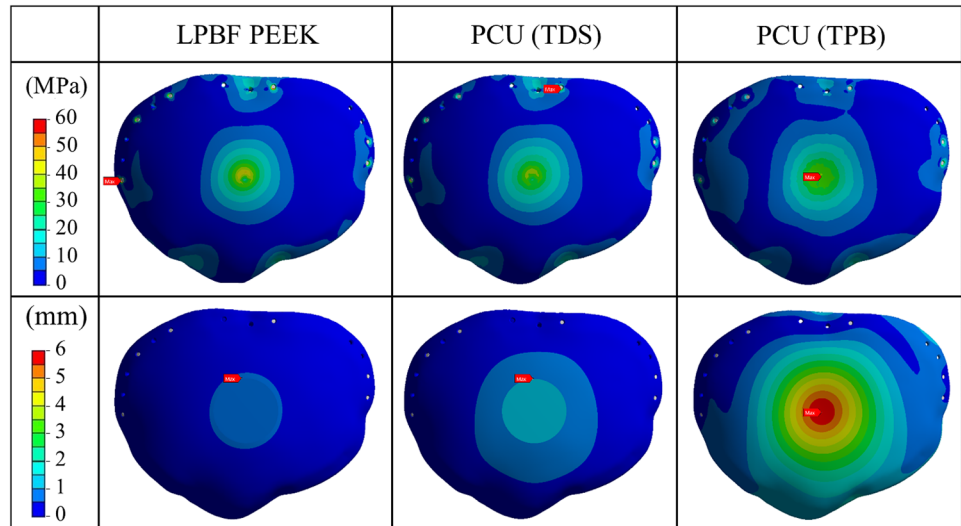


**Table 5** Equivalent von Mises stress on the screws and contact point with punch at 50 N (values are in MPa)

	L1	L4	L6	T3	R2	R1	Punch
LPBF PEEK	7.96	5.87	4.50	3.51	6.32	7.24	5.57
PCU TDS	7.33	5.50	4.23	3.25	6.06	6.75	5.62
PCU TPB	5.65	4.21	3.18	3.33	4.54	4.77	5.05

**Table 6** Equivalent von Mises stress on the screws and contact point with punch at 500 N (values are in MPa)

	L1	L4	L6	T3	R2	R1	Punch
LPBF PEEK	63.6	42.0	41.2	62.9	32.1	42.7	46.2
PCU TDS	43.9	28.9	27.0	44.2	24.4	30.3	38.7
PCU TPB	35.6	21.3	18.9	28.1	23.6	30.3	35.6

PEEK solution. Specifically, the expected deformation at 500 N increases by 38% moving from LPBF PEEK to TDS PCU (i.e. from 0.82 to 1.32 mm). This finding was expected in light of the Young moduli of the two materials reported in Table 1. It is worth highlighting that the FEA displacement calculated in the case of TDS PCU is lower than 3 mm, which is the assumed deflection limit defined by [71] for these applications. This is of great relevance since the maximum deformation during usage is a crucial aspect to ensure patient safety. The results of FEA run with TDS PCU properties would thus suggest that this combination of design and material is suitable for being implanted.

Nevertheless, a completely different conclusion is drawn if considering the 3D-printed TPB properties. In fact, the results of experimental density measures, equal to  $0.966 \pm 0.002 \text{ g/cm}^3$ , show that the density of the 3D-printed material is 20% lower than the TDS, equal to  $1.22 \text{ g/cm}^3$ . This result indicates that internal voids were generated by the printing process. The difference in mechanical properties is even more relevant, with a decrease of approximately 70% in both flexural modulus and stress. Indeed, Hentschel

et al. printed tensile specimens with the APF, and found a clear relationship between density and tensile properties [72]. Nevertheless the observed drop of mechanical properties is only partially attributable to the difference in density. Arguably, the APF process determines also a sub-optimal adhesion between material drops. It is worth mentioning that the chamber temperature used for processing (i.e.  $120 \text{ }^\circ\text{C}$ ) is the maximum reachable by this printer. Higher temperatures would possibly allow for a more efficient bonding between the polymer chains. The differences in mechanical properties between the TDS and the experimental observations have also a dramatic impact on the FEA. In fact, the curves in Fig. 14 show that the 3D-printed material does not reach the maximum load of 500 N even for a displacement of 6 mm, namely twice the upper limit to deflection. As reported in Table 7, a significant difference in displacement can be observed also at lower values of load. It can be observed that only the plate FEA run with TDS properties reached 500 N without surpassing 3 mm of displacement. The FEA run with 3D-printed TPB properties, respect the limits until 300 N and the two printed plates until 200 N.

**Table 7** Comparison between displacements calculated by FEA with different PCU properties (3D-printed TPB and TDS) and experimental observations (values in mm)

Load (N)	EXP PCU (25% sup.)	EXP PCU (50% sup.)	FEA PCU (3DP TPB)	FEA PCU (TDS)
50	0.47	0.45	0.43	0.17
100	1.06	0.94	0.82	0.30
200	2.99	2.31	1.70	0.56
300	–	–	2.81	0.81
500	–	–	–	1.32

A further decrease in bearable load is observed in the experimental tests on the cranial plates printed by APF. In fact, the results in Fig. 14 and Table 7 show that the deflection of the real implant is significantly higher than the value calculated by FEA. This decrease in mechanical properties is possibly attributable to the particular shape of the implant. In fact, while the specimens for TPB are planar, the curvature of the cranial plate means that the bottom surface is not in contact with the building plate. Since non-full support structures are used, the effect of gravity might further affect the density and adhesion of the material, determining a supplementary loss in stiffness. In Fig. 16, a magnification of the cut sections of the 3D-printed PCU plate shows the formation of several voids. This hypothesis is supported by the comparison between the results obtained on the two replicas of the implant. In fact, it can be seen that more dense support structures allow for reducing the deflection of the cranial plate. This finding highlights the importance of researching a solvable support material compatible with PCU. Such a material would allow for fully dense support to

the deposited material during printing and could be removed without damaging the part at the end of the process.

It is worth mentioning that the present study considered a single geometry of the implant, which was originally designed for PEEK. Significant improvements in maximum deformation and stress could be undoubtedly achieved by optimising the design for PCU. For example, small variations in the plate thickness may considerably affect the mechanical response of the part [59].

Also, in line with the existing literature, a static load of 500 N was investigated to simulate the response of the system in case of impact. Nonetheless, the elastomeric properties of PCU suggest that the energy absorption under dynamic loads might considerably differ from the quasi-static behaviour. Further studies will be thus dedicated to experimentally characterising the impact resistance of APF-printed PCU implants.

## 5 Conclusions

The present study explored, for the first time, the possibility to realise a cranial plate in PCU via APF 3D-printing process. This opens new marvellous opportunities for the on-demand manufacturing of patient-specific implants in a clean hospital environment. A FEM to estimate the mechanical behaviour of these implants has been presented and validated. Additionally, one of the most critical area for evaluating implant performance is the implant-screw interface, which future studies should be focused.

Overall, the results suggest that, due to the lower stiffness of PCU, a redesign of the cranial implant is needed to limit deformations under the maximum expected loads.

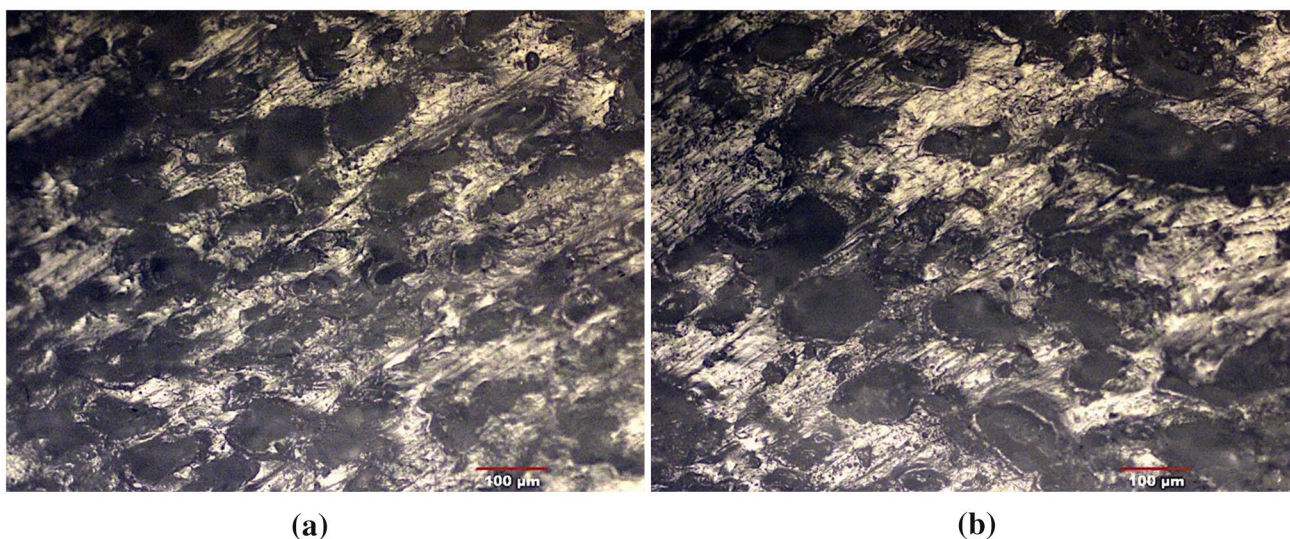


**Fig. 16** Picture of the section of the plate, observed at the microscope, for plates with support at **a** 25%, **b** 50%

Experimental findings also highlight that the 3D-printing process determines a considerable loss in density and stiffness with respect to the TDS material properties, which are acquired from injection molded specimens (i.e. more dense). It is thus crucial to include the effect of the process within the material model used for calculation to avoid incorrect evaluations.

Experimental observations show a significant influence of support design on the mechanical performance of the manufactured plate. This highlights the importance to find suitable support materials compatible with PCU to realise fully dense support structures. Higher build chamber temperatures and further fine-tuning of process parameters could also improve the final properties of the implant.

**Acknowledgements** The authors would like to thank Arburg Gmbh and Arburg Italia for the technical support. Special thanks go to Ph.D. Davide Cocchi for supporting the present work.

**Funding** Open access funding provided by Alma Mater Studiorum - Università di Bologna within the CRUI-CARE Agreement.

**Open Access** This article is licensed under a Creative Commons Attribution 4.0 International License, which permits use, sharing, adaptation, distribution and reproduction in any medium or format, as long as you give appropriate credit to the original author(s) and the source, provide a link to the Creative Commons licence, and indicate if changes were made. The images or other third party material in this article are included in the article's Creative Commons licence, unless indicated otherwise in a credit line to the material. If material is not included in the article's Creative Commons licence and your intended use is not permitted by statutory regulation or exceeds the permitted use, you will need to obtain permission directly from the copyright holder. To view a copy of this licence, visit <http://creativecommons.org/licenses/by/4.0/>.

## References

- Alkhaibary A, Alharbi A, Alnefaie N, Almubarak AO, Aloraidi A, Khairy S (2020) Cranioplasty: a comprehensive review of the history, materials, surgical aspects, and complications. *World Neurosurg* 139:445–452. <https://doi.org/10.1016/j.wneu.2020.04.211>
- Aydin S, Kucukyuruk B, Abuzayed B, Aydin S, Sanus GZ (2011) Cranioplasty: review of materials and techniques. *J Neurosci Rural Pract* 02:162–167. <https://doi.org/10.4103/0976-3147.83584>. (Number: 2)
- Alasseri N, Alasraj A (2020) Patient-specific implants for maxillofacial defects: challenges and solutions. *Maxillofac Plast Reconstr Surg* 42:15. <https://doi.org/10.1186/s40902-020-00262-7>
- Ghantous Y, Nashef A, Mohanna A, Abu-El-naaj I (2020) Three-dimensional technology applications in maxillofacial reconstructive surgery: current surgical implications. *Nanomaterials* 10:2523. <https://doi.org/10.3390/nano10122523>. (Number: 12)
- Maniar RN, Singhi T (2014) Patient specific implants: scope for the future. *Curr Rev Musculoskelet Med* 7:125–130. <https://doi.org/10.1007/s12178-014-9214-2>
- Jindal S, Manzoor F, Haslam N, Mancuso E (2021) 3d printed composite materials for craniofacial implants: current concepts, challenges and future directions. *Int J Adv Manuf Technol* 112:635–653. <https://doi.org/10.1007/s00170-020-06397-1>
- Geringer J, Tatkiwicz W, Rouchouse G (2011) Wear behavior of paek, poly(aryl-ether-ketone), under physiological conditions, outlooks for performing these materials in the field of hip prosthesis. *Wear* 271:2793–2803. <https://doi.org/10.1016/j.wear.2011.05.034>
- Ridwan-Pramana A, Marcián P, Borák L, Narra N, Forouzanfar T, Wolff J (2016) Structural and mechanical implications of PMMA implant shape and interface geometry in cranioplasty—a finite element study. *J Cranio-Maxillofac Surg* 44:34–44. <https://doi.org/10.1016/j.jcms.2015.10.014>
- Ford AC (2019) Mechanical evaluation of polycarbonate polyurethane for long-term orthopedic implant applications. PhD thesis, University of California, Berkeley
- McElhaney JH, Fogle JL, Melvin JW, Haynes RR, Roberts VL, Alem NM (1970) Mechanical properties of cranial bone. *J Biomech* 3:495–511. [https://doi.org/10.1016/0021-9290\(70\)90059-X](https://doi.org/10.1016/0021-9290(70)90059-X)
- Tuusa SM-R, Peltola MJ, Tirri T, Puska MA, Røyttä M, Aho H, Sandholm J, Lassila LVJ, Vallittu PK (2008) Reconstruction of critical size calvarial bone defects in rabbits with glass-fiber-reinforced composite with bioactive glass granule coating. *J Biomed Mater Res B Appl Biomater* 84B:510–519. <https://doi.org/10.1002/jbm.b.30898>
- Souza Leão R, Maior JRS, Araújo Lemos CA, Egito Vasconcelos BC, Montes M, Pellizzer EP, Moraes SLD (2018) Complications with PMMA compared with other materials used in cranioplasty: a systematic review and meta-analysis. *Braz Oral Res* 32:31. <https://doi.org/10.1590/1807-3107bor-2018.vol32.0031>
- Kobayashi K, Yukiue T, Yoshida H, Tsuboi N, Takahashi Y, Makino K, Kimura R, Mizuta R, Sasada S, Ogawa T, Nagayama N, Yasuhara T, Date I (2021) Ultra-high-molecular-weight polyethylene (uhmwpe) wing method for strong cranioplasty. *Neurologia medico-chirurgica* 61:2021–0032. <https://doi.org/10.2176/nmc.0a.2021-0032>
- Feng X, Yu H, Liu H, Yu X, Feng Z, Bai S, Zhao Y (2019) Three-dimensionally-printed polyether-ether-ketone implant with a cross-linked structure and acid-etched microporous surface promotes integration with soft tissue. *Int J Mol Sci* 20:3811. <https://doi.org/10.3390/ijms20153811>
- Punchak M, Chung LK, Lagman C, Bui TT, Lazareff J, Rezzadeh K, Jarrahy R, Yang I (2017) Outcomes following polyetheretherketone (peek) cranioplasty: systematic review and meta-analysis. *J Clin Neurosci* 41:30–35. <https://doi.org/10.1016/j.jocn.2017.03.028>
- Wang M, Bhardwaj G, Webster T (2017) Antibacterial properties of PEKK for orthopedic applications. *Int J Nanomed* 12:6471–6476. <https://doi.org/10.2147/IJN.S134983>
- Adamzyk C, Kachel P, Hoss M, Gremse F, Modabber A, Hölzle F, Tolba R, Neuss S, Lethaus B (2016) Bone tissue engineering using polyetherketoneketone scaffolds combined with autologous mesenchymal stem cells in a sheep calvarial defect model. *J Cranio-Maxillofac Surg* 44:985–994. <https://doi.org/10.1016/j.jcms.2016.04.012>
- Inyang AO, Vaughan CL (2020) Functional characteristics and mechanical performance of PCU composites for knee meniscus replacement. *Materials* 13:1886. <https://doi.org/10.3390/ma13081886>
- Bracco P, Zanetti M, Cipriani E, Costa L (2010) Characterization of a polycarbonate-urethane elastomer for orthopedic applications. 2008:1191
- Cipriani E, Bracco P, Kurtz SM, Costa L, Zanetti M (2013) In-vivo degradation of poly(carbonate-urethane) based spine implants. *Polym Degrad Stab* 98:1225–1235. <https://doi.org/10.1016/j.polymdegradstab.2013.03.005>

21. Elsner JJ, McKeon BP (2017) Orthopedic application of polycarbonate urethanes: a review. *Tech Orthop* 32:132–140. <https://doi.org/10.1097/BTO.0000000000000216>
22. Chang SCN, Tobias G, Roy AK, Vacanti CA, Bonassar LJ (2003) Tissue engineering of autologous cartilage for craniofacial reconstruction by injection molding. *Plast Reconstr Surg* 112:793–799. <https://doi.org/10.1097/01.PRS.0000069711.31021.94>
23. Wolfaardt JF, Coss P (1996) An impression and cast construction technique for implant-retained auricular prostheses. *J Prosthet Dent* 75:45–49. [https://doi.org/10.1016/S0022-3913\(96\)90415-1](https://doi.org/10.1016/S0022-3913(96)90415-1)
24. Stansbury JW, Idacavage MJ (2016) 3d printing with polymers: challenges among expanding options and opportunities. *Dent Mater* 32:54–64. <https://doi.org/10.1016/j.dental.2015.09.018>
25. Scolozzi P, Martinez A, Jaques B (2007) Complex orbito-fronto-temporal reconstruction using computer-designed peek implant. *J Craniofac Surg* 18:224–228. <https://doi.org/10.1097/01.scs.0000249359.56417.7e>
26. Alemayehu DG, Zhang Z, Tahir E, Gateau D, Zhang D-F, Ma X (2021) Preoperative planning using 3d printing technology in orthopedic surgery. *BioMed Res Int*. <https://doi.org/10.1155/2021/7940242>
27. Battaglia S, Badiali G, Cercenelli L, Bortolani B, Marcelli E, Cipriani R, Contedini F, Marchetti C, Tarsitano A (2019) Combination of cad/cam and augmented reality in free fibula bone harvest. *Plast Reconstr Surg Glob Open* 7:2510. <https://doi.org/10.1097/GOX.00000000000002510>
28. Battaglia S, Ricotta F, Maiolo V, Savastio G, Contedini F, Cipriani R, Bortolani B, Cercenelli L, Marcelli E, Marchetti C, Tarsitano A (2019) Computer-assisted surgery for reconstruction of complex mandibular defects using osteomyocutaneous microvascular fibular free flaps: Use of a skin paddle-outlining guide for soft-tissue reconstruction. a technical report. *J Cranio-Maxillofac Surg* 47:293–299. <https://doi.org/10.1016/j.jcms.2018.11.018>
29. Gauci M-O (2022) Patient-specific guides in orthopedic surgery. *Orthop Traumatol Surg Res* 108:103154. <https://doi.org/10.1016/j.otsr.2021.103154>
30. Hoang D, Perrault D, Stevanovic M, Ghiassi A (2016) Surgical applications of three-dimensional printing: a review of the current literature how to get started. *Ann Transl Med* 4:456–456. <https://doi.org/10.21037/atm.2016.12.18>
31. Schiavina R, Bianchi L, Borghesi M, Chessa F, Cercenelli L, Marcelli E, Brunocilla E (2019) Three-dimensional digital reconstruction of renal model to guide preoperative planning of robot-assisted partial nephrectomy. *Int J Urol* 26:931–932. <https://doi.org/10.1111/iju.14038>
32. Bianchi L, Barbaresi U, Cercenelli L, Bortolani B, Gaudiano C, Chessa F, Angiolini A, Lodi S, Porreca A, Bianchi FM, Casablanca C, Ercolino A, Bertaccini A, Golfieri R, Marcelli E, Schiavina R (2020) The impact of 3d digital reconstruction on the surgical planning of partial nephrectomy: a case-control study. still time for a novel surgical trend? *Clin Genitourin Cancer* 18:669–678. <https://doi.org/10.1016/j.clgc.2020.03.016>
33. Bonda DJ, Manjila S, Selman WR, Dean D (2015) The recent revolution in the design and manufacture of cranial implants. *Neurosurgery* 77:814–824. <https://doi.org/10.1227/NEU.0000000000000899>
34. Honigmann P, Sharma N, Okolo B, Popp U, Msallem B, Thieringer FM (2018) Patient-specific surgical implants made of 3d printed peek: material, technology, and scope of surgical application. *Biomed Res Int* 2018:1–8. <https://doi.org/10.1155/2018/4520636>
35. Schmidt M, Pohle D, Rechtenwald T (2007) Selective laser sintering of peek. *CIRP Ann* 56:205–208. <https://doi.org/10.1016/j.cirp.2007.05.097>
36. Ghita OR, James E, Trimble R, Evans KE (2014) Physico-chemical behaviour of poly (ether ketone) (PEK) in high temperature laser sintering (HT-LS). *J Mater Process Technol* 214:969–978. <https://doi.org/10.1016/j.jmatprotec.2013.11.007>
37. Sharma N, Aghlmandi S, Dalcanale F, Seiler D, Zeilhofer H-F, Honigmann P, Thieringer FM (2021) Quantitative assessment of point-of-care 3d-printed patient-specific polyetheretherketone (peek) cranial implants. *Int J Mol Sci* 22:8521. <https://doi.org/10.3390/ijms22168521>
38. Sharma N, Aghlmandi S, Cao S, Kunz C, Honigmann P, Thieringer FM (2020) Quality characteristics and clinical relevance of in-house 3d-printed customized polyetheretherketone (peek) implants for craniofacial reconstruction. *J Clin Med* 9:2818. <https://doi.org/10.3390/jcm9092818>
39. Petersmann S, Smith JA, Schäfer U, Arbeiter F (2023) Material extrusion-based additive manufacturing of polyetheretherketone cranial implants: mechanical performance and print quality. *J Market Res* 22:642–657. <https://doi.org/10.1016/j.jmrt.2022.11.143>
40. Singh S, Prakash C, Ramakrishna S (2019) 3d printing of polyether-ether-ketone for biomedical applications. *Eur Polym J* 114:234–248. <https://doi.org/10.1016/j.eurpolymj.2019.02.035>
41. Wu W, Geng P, Li G, Zhao D, Zhang H, Zhao J (2015) Influence of layer thickness and raster angle on the mechanical properties of 3d-printed peek and a comparative mechanical study between peek and abs. *Materials* 8:5834–5846. <https://doi.org/10.3390/ma8095271>
42. Dey A, Eagle INR, Yodo N (2021) A review on filament materials for fused filament fabrication. *J Manuf Mater Process* 5:69. <https://doi.org/10.3390/jmmp5030069>
43. (2018) Extrusion-based additive manufacturing process for producing flexible parts. *J Braz Soc Mech Sci Eng* 40:143. <https://doi.org/10.1007/s40430-018-1068-x>
44. Netto JMJ, Idogava HT, Santos LEF, Castro Silveira Z, Romio P, Alves JL (2021) Screw-assisted 3d printing with granulated materials: a systematic review. *Int J Adv Manuf Technol* 115:2711–2727. <https://doi.org/10.1007/s00170-021-07365-z>
45. Shaik YP, Schuster J, Shaik A (2021) A scientific review on various pellet extruders used in 3d printing fdm processes. *OALib* 08:1–19. <https://doi.org/10.4236/oalib.1107698>
46. Gaub H (2016) Customization of mass-produced parts by combining injection molding and additive manufacturing with industry 4.0 technologies. *Reinf Plast* 60:401–404. <https://doi.org/10.1016/j.repl.2015.09.004>
47. Minetola P, Calignano F, Galati M (2020) Comparing geometric tolerance capabilities of additive manufacturing systems for polymers. *Addit Manuf* 32:101103. <https://doi.org/10.1016/j.addma.2020.101103>
48. Pinter P, Baumann S, Lohr C, Heuer A, Englert L, Weidenmann KA (2020) Mechanical properties of additively manufactured polymer samples using a piezo controlled injection molding unit and fused filament fabrication compared with a conventional injection molding process, pp 2219–2227
49. Pollack SAI (2019) historical developments, process types and material considerations. Springer, pp 1–22
50. Hentschel L, Kynast F, Petersmann S, Holzer C, Gonzalez-Gutierrez J (2020) Processing conditions of a medical grade poly(methyl methacrylate) with the arburg plastic freeforming additive manufacturing process. *Polymers* 12:2677. <https://doi.org/10.3390/polym12112677>
51. Ahlinder A, Charlson S, Fuoco T, Soulestin J, Finne-Wistrand A (2020) Minimise thermo-mechanical batch variations when processing medical grade lactide based copolymers in additive manufacturing. *Polym Degrad Stab* 181:109372. <https://doi.org/10.1016/j.polymdgradstab.2020.109372>

52. Hirsch A, Dalmer C, Moritzer E (2021) Investigation of plastic freeformed, open-pored structures with regard to producibility, reproducibility and liquid permeability. Springer 1:112–129. [https://doi.org/10.1007/978-3-030-54334-1\\_9](https://doi.org/10.1007/978-3-030-54334-1_9)
53. Welsh NR, Malcolm RK, Devlin B, Boyd P (2019) Dapivirine-releasing vaginal rings produced by plastic freeforming additive manufacturing. *Int J Pharm* 572:118725. <https://doi.org/10.1016/j.ijpharm.2019.118725>
54. Zhang B, Nasereddin J, McDonagh T, Zeppelin D, Gleadall A, Alqahtani F, Bibb R, Belton P, Qi S (2021) Effects of porosity on drug release kinetics of swellable and erodible porous pharmaceutical solid dosage forms fabricated by hot melt droplet deposition 3d printing. *Int J Pharm* 604:120626. <https://doi.org/10.1016/j.ijpharm.2021.120626>
55. Pawelczyk L (2021) Making the impossible possible: the free-former in 3D printing. [https://www.medicalplasticsnews.com/medical-plastics-industry-insights/medical-plastics-3d-printing-insights/making-the-impossible-possible\\_1/](https://www.medicalplasticsnews.com/medical-plastics-industry-insights/medical-plastics-3d-printing-insights/making-the-impossible-possible_1/)
56. Halabi FE, Rodriguez JF, Rebolledo L, Hurtós E, Doblaré M (2011) Mechanical characterization and numerical simulation of polyether-ether-ketone (peek) cranial implants. *J Mech Behav Biomed Mater* 4:1819–1832. <https://doi.org/10.1016/j.jmbbm.2011.05.039>
57. Garcia-Gonzalez D, Jayamohan J, Sotiropoulos SN, Yoon S-H, Cook J, Siviour CR, Arias A, Jérusalem A (2017) On the mechanical behaviour of peek and ha cranial implants under impact loading. *J Mech Behav Biomed Mater* 69:342–354. <https://doi.org/10.1016/j.jmbbm.2017.01.012>
58. Wan Z, Huang C, Li Y, Wan C, Zhong R (2018) The evaluation of bio-mechanical properties of four different skull implants by finite element methods. *Biomed Res* 29:1879–1884. <https://doi.org/10.4066/biomedicalresearch.29-18-139>
59. Marcián P, Narra N, Borák L, Chamrad J, Wolff J (2019) Bio-mechanical performance of cranial implants with different thicknesses and material properties: a finite element study. *Comput Biol Med* 109:43–52. <https://doi.org/10.1016/j.compbimed.2019.04.016>
60. Kodym O, Španel M, Herout A (2021) Deep learning for cranioplasty in clinical practice: Going from synthetic to real patient data. *Comput Biol Med* 137:104766. <https://doi.org/10.1016/j.compbimed.2021.104766>
61. Li J, Campe G, Pepe A, Gsaxner C, Wang E, Chen X, Zefferer U, Tödting M, Krall M, Deutschmann H, Schäfer U, Schmalstieg D, Egger J (2021) Automatic skull defect restoration and cranial implant generation for cranioplasty. *Med Image Anal* 73:102171. <https://doi.org/10.1016/j.media.2021.102171>
62. Li J, Ellis DG, Pepe A, Gsaxner C, Aizenberg MR, Kleesiek J, Egger J (2022) Back to the roots: reconstructing large and complex cranial defects using an image-based statistical shape model. <http://arxiv.org/abs/2204.05703>
63. Biomedical D (2020) Bionate®Thermoplastic polycarbonate polyurethane . [https://www.dsm.com/content/dam/dsm/biomedical/en\\_us/documents/document-bionate-pcu-productsheet.pdf](https://www.dsm.com/content/dam/dsm/biomedical/en_us/documents/document-bionate-pcu-productsheet.pdf)
64. Geary C, Birkinshaw C, Jones E (2008) Characterisation of bionate polycarbonate polyurethanes for orthopaedic applications. *J Mater Sci Mater Med* 19:3355–3363. <https://doi.org/10.1007/s10856-008-3472-8>
65. Khan I, Smith N, Jones E, Finch DS, Cameron RE (2005) Analysis and evaluation of a biomedical polycarbonate urethane tested in an in vitro study and an ovine arthroplasty model. part ii: in vivo investigation. *Biomaterials* 26:633–643. <https://doi.org/10.1016/j.biomaterials.2004.02.064>. (Number: 6)
66. Tienen TG, Hannink G, Buma P (2009) Meniscus replacement using synthetic materials. *Clin Sports Med* 28:143–156. <https://doi.org/10.1016/j.csm.2008.08.003>
67. Formlabs: Standard Material Data Sheet (2017). <https://formlabs-media.formlabs.com/datasheets/Standard-DataSheet.pdf>
68. Mele M, Pisaneschi G, Campana G, Zucchelli A, Ciotti M (2022) Effect of selected process parameters on dimensional accuracy in arburg plastic freeforming. *Rapid Prototyp J* 28:1677–1689. <https://doi.org/10.1108/RPJ-05-2021-0109>
69. Hoskins TJ, Dearn KD, Kukureka SN (2018) Mechanical performance of peek produced by additive manufacturing. *Polym Test* 70:511–519. <https://doi.org/10.1016/j.polymertesting.2018.08.008>
70. Ghali NNA, Littlei EG (2008) Determination of the mechanical properties of bionate 80a and bionate 75d for the stress analysis of cushion form bearings, 222, 683–694 . <https://doi.org/10.1243/09544119JEIM372>
71. Ulmeanu M-E, Doicin C-V, Mates I, Murzac R, Davitoiu D (2001) Impact FEA simulation and analysis of custom-made cranial implants. *Revista de Chimie* 71:367–376. <https://doi.org/10.37358/RC.20.3.8010>
72. Hentschel L, Petersmann S, Gonzalez-Gutierrez J, Kynast F, Schäfer U, Arbeiter F, Holzer C (2023) Parameter optimization of the arburg plastic freeforming process by means of a design of experiments approach. *Adv Eng Mater* 25:2200279. <https://doi.org/10.1002/adem.202200279>

**Publisher's Note** Springer Nature remains neutral with regard to jurisdictional claims in published maps and institutional affiliations.